

# Local vibration of an elastic plate and zero-group velocity Lamb modes

Claire Prada,<sup>a)</sup> Dominique Clorennec, and Daniel Royer

Laboratoire Ondes et Acoustique, ESPCI-Université Paris 7-CNRS UMR 7587, 10 rue Vauquelin, 75231 Paris Cedex 05- France

(Received 26 October 2007; revised 6 March 2008; accepted 10 April 2008)

Elastic plates or cylinders can support guided modes with zero group velocity (ZGV) at a nonzero value of the wave number. Using laser-based ultrasonic techniques, we experimentally investigate some fascinating properties of these ZGV modes: resonance and ringing effects, backward wave propagation, interference between backward and forward modes. Then, the conditions required for the existence of ZGV Lamb modes in isotropic plates are discussed. It is shown that these modes appear in a range of Poisson's ratio about the value for which the cutoff frequency curves of modes belonging to the same family intercept, i.e., for a bulk wave velocity ratio equal to a rational number. An interpretation of this phenomenon in terms of a strong repulsion between a pair of modes having a different parity in the vicinity of the cutoff frequencies is given. Experiments performed with materials of various Poisson's ratio demonstrate that the resonance spectrum of an unloaded elastic plate, locally excited by a laser pulse, is dominated by the ZGV Lamb modes.

© 2008 Acoustical Society of America. [DOI: 10.1121/1.2918543]

PACS number(s): 43.40.Dx, 43.20.Mv, 43.35.Yb [RLW]

Pages: 203–212

## I. INTRODUCTION

Material characterization using elastic waves is an active domain of applied research. Ultrasonic thickness gauges, which operate by measuring the round-trip interval for a longitudinal wave pulse to traverse the plate or wall under inspection, are routinely used for industrial process control.<sup>1</sup> To be accurate, this pulse echo method requires the use of high frequency piezoelectric transducers for launching bulk waves having wavelength much smaller than the plate thickness. It suffers limitations on rough or curved surfaces and also due to the significant increase of attenuation with frequency. Guided waves emerged as an alternative to this conventional point-by-point nondestructive evaluation for fast inspection of large structures.<sup>2</sup> In a specific approach, developed simultaneously with noncontact laser ultrasonics techniques, the dispersion characteristics of some Lamb modes are exploited for extracting the mechanical properties or the thickness of a given plate. It needs lower frequency waves but requires many local measurements of the normal displacement along several wavelengths on the surface of the plate.<sup>3</sup> Consequently, this method is slow and limited to homogeneous plates.

Resonance techniques have the advantage to operate at lower frequencies (bulk wavelength of the order of plate thickness). Among them, the “impact echo” method has been developed for civil engineering applications.<sup>4</sup> The vibration excited by a point-like shock is detected close to the impact. This local investigation technique is, however, limited to thick structures. For ultrasonic applications, the use of electro-magneto-acoustic transducers allows noncontact evaluation of metal sheets.<sup>5</sup> Like in the pulse echo technique,

the sheet is assumed to be uniform over a large number of thicknesses leading to a poor spatial resolution. For a long time, engineers considered only bulk wave propagation in the direction normal to the plate and did not pay much attention to the guided nature of elastic waves propagating in the plate. In many cases, the role of Lamb modes is not significant because the lateral dimensions of the source are larger than the Lamb mode wavelength. However, in the case of sources having dimensions of the order of the plate thickness, Lamb modes are generated and must be considered.

The propagation of elastic waves in a plate or in a cylindrical shell has been extensively investigated during the last century. The dispersive properties of guided modes in a free standing plate are well understood.<sup>6,7</sup> Fifty years ago, Tolstoy and Usdin pointed out that for the  $S_1$  Lamb mode, group velocity vanishes at a particular point of the dispersion curve.<sup>8</sup> They also predicted that this zero group velocity (ZGV) point “must be associated with a sharp continuous wave resonance and ringing effects.” However, they did not discuss the manner to generate such a resonance. Although the derivation of the transient response of a plate to a point source was achieved by Weaver and Pao in 1982,<sup>9</sup> it is only recently that the importance of zero group velocity Lamb modes in the measurements with short distances between excitation and detection points has been pointed out through some numerical studies<sup>10</sup> and experimental works.<sup>11–16</sup>

Since at a ZGV point the phase velocity and then the wavelength remains finite, the energy can be locally trapped in the source area without any transfer to the adjacent medium. In a narrow range of frequency above this ZGV point and for a given energy propagation direction (from the source to the observation point), two waves can propagate spatially with opposite phase velocities and wave vectors. This backward propagation has been experimentally ob-

<sup>a)</sup>Author to whom correspondence should be addressed. Electronic mail: claire.prada-julia@espci.fr.

served in elastic cylinders or plates immersed in water.<sup>17,18</sup> In these conditions, the surrounding fluid causes a large damping of the ZGV resonance.

Using broadband, focusing air-coupled transducers, Holland and Chimenti<sup>11</sup> found that the mechanical softening due to this resonance allows efficient transmission of airborne sound waves through a thick plate. However, laser based ultrasonic techniques, developed for noncontact evaluation of materials, provide an invaluable tool for investigating these ZGV resonances. Direct evidence of this phenomenon was observed by Prada, Balogun, and Murray, with an amplitude modulated laser diode and a Michelson interferometer.<sup>13,14</sup> By scanning the modulation frequency, they show that the thermoelastic source is efficiently coupled to the first symmetric ( $S_1$ ) Lamb mode at the ZGV point and that the same effect can be observed for the second antisymmetric ( $A_2$ ) Lamb mode. Recently, the “ringing effect,” predicted by Tolstoy and Usdin, has been excited by a laser pulse and optically detected in the time domain.<sup>15</sup> With the same experimental setup, we demonstrated that these resonances can be used for locally measuring the mechanical properties of isotropic materials.<sup>16</sup>

This paper is organized as the following: The nature of ZGV Lamb modes is investigated through laser based ultrasonic (LBU) measurements in Sec. II. These experiments, performed on the  $S_1$ -Lamb mode, give a clear evidence of the propagation of a backward wave. The conditions of existence of ZGV-Lamb modes versus Poisson’s ratio are established in Sec. III. An interpretation, valid for all ZGV modes in terms of a strong repulsion between a pair of modes in the vicinity of the cutoff frequencies is given. In Sec. IV, it is shown that the local vibration spectrum of an elastic plate is dominated by the ZGV resonances and that these resonances can be exploited for locally measuring the mechanical properties of isotropic materials in plates and hollow cylinders.

## II. EXPERIMENTAL EVIDENCE OF $S_1$ ZGV LAMB MODE RESONANCE AND BACKWARD WAVE

Before discussing the whole set of ZGV Lamb modes, we investigate the fascinating behavior of these particular modes through measurements and analysis of the  $S_1$  ZGV mode generated and detected on a Duralumin plate.

Lamb modes (frequency  $f$ , wavelength  $\lambda$ ) are represented by a set of curves giving the angular frequency  $\omega$  of each symmetric ( $S$ ) and antisymmetric ( $A$ ) mode versus the wave number  $k$ . Figure 1 shows the dispersion curve of the lower order modes for a Duralumin plate of thickness  $d$  (longitudinal wave velocity  $V_L=6.34$  km/s and transverse velocity  $V_T=3.14$  km/s). We have plotted the variations of the frequency thickness product  $fd=\omega d/2\pi$  versus the thickness to wavelength ratio  $d/\lambda=kd/2\pi$ . The  $A_0$  and  $S_0$  modes exhibit free propagation to zero frequency, whereas higher order modes admit a cutoff frequency  $f_c$  when the wave number  $k$  approaches zero. Conversely to other modes, the first order symmetric ( $S_1$ ) mode exists for small wave numbers at values of  $fd$  below the cutoff frequency ( $f_c d=V_T=3.14$  MHz mm). The slope of the dispersion curve is nega-

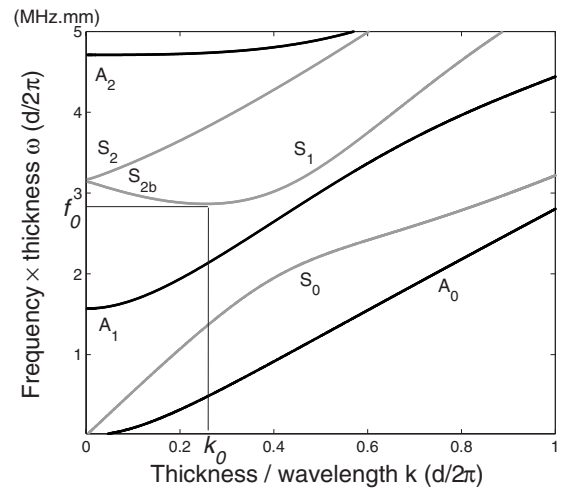


FIG. 1. Dispersion curves for a Duralumin plate of thickness  $d$  and bulk wave velocities equal to  $V_L=6.34$  km/s and  $V_T=3.14$  km/s. Vertical scale:  $fd=\omega d/2\pi$ , horizontal scale:  $d/\lambda=kd/2\pi$ .

tive and the frequency begins to increase at a point ( $k_0 d=1.58, f_0 d=2.866$  MHz mm) where the frequency undergoes a minimum and then the group velocity  $d\omega/dk$  vanishes. In contrast with the cutoff modes, at this ZGV point, the  $S_1$ -mode phase velocity remains finite ( $V_0=11.25$  km/s). In a narrow range between this minimum frequency  $f_0$  and the cutoff frequency  $f_c$ , the dispersion curve is double valued. For wave numbers  $k < k_0$ , phase and group velocities are of opposite signs: backward propagation occurs. In the literature,<sup>17,19,20</sup> the negative slope branch is classified as part of the  $S_2$  mode and is labeled  $S_{2b}$ , where  $b$  stands for “backward wave.” As shown in Kaduchak *et al.*,<sup>19</sup> the distinction between  $S_1$  and  $S_{2b}$  modes appears clearly by solving the Rayleigh Lamb equation for a complex wave number. Indeed, the  $S_{2b}$  branch is connected to the  $S_2$  branch by a purely imaginary branch. Furthermore, for a water loaded plate, due to leakage, the two branches  $S_1$  and  $S_{2b}$  are separate.

For nondissipation, both in the material and across the waveguide boundaries, it has been shown that the energy velocity is equal to the group velocity.<sup>21</sup> At the frequency  $f_0$ , the energy of the  $S_1$ -Lamb mode is trapped under the source resulting in ringing and resonance phenomena. This behavior is observed in solids having a Poisson’s ratio  $\nu < 0.45$ , i.e., for most usual materials.

Since any mechanical contact with the plate is responsible for an energy leakage, these effects are not easily observed with standard piezoelectric transducers. On the contrary, laser-based ultrasonic (LBU) techniques are appropriate for investigating ZGV modes. They eliminate coupling issues in the generation and detection of the waves, and their high temporal resolution enables studying the resonance spectrum of the plate over a large frequency range.

### A. Experimental setup

As shown in Fig. 2, Lamb waves were generated by a Q-switched Nd:YAG (yttrium aluminium garnet) laser providing pulses having a 20 ns duration and 4 mJ of energy. The spot diameter of the unfocused beam is equal to 1 mm.

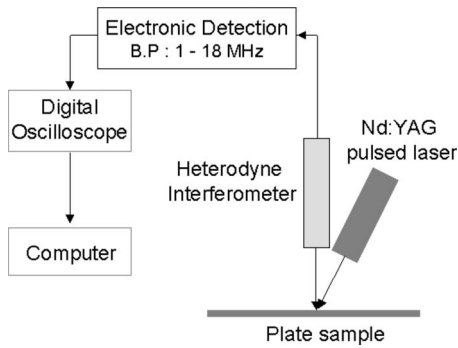


FIG. 2. Experimental setup.

Local vibrations were measured by a heterodyne interferometer equipped with a 100 mW frequency doubled Nd:YAG laser (optical wavelength  $\Lambda=532$  nm). This interferometer is sensitive to any phase shift  $\Delta\phi$  along the path of the optical probe beam, and then to the mechanical displacement  $u$  normal to the surface. As previously shown,<sup>22</sup> the calibration factor (10 nm/V), deduced from the phase modulation  $\Delta\phi = 4\pi u/\Lambda$  of the reflected beam, was constant over the detection bandwidth (50 kHz–20 MHz). Signals detected by the optical probe were fed into a digital sampling oscilloscope and transferred to a computer.

As discussed in Balogun *et al.*,<sup>14</sup> for a laser spot diameter equal to half the ZGV mode wavelength  $\lambda$ , the efficiency of the thermoelastic generation of this mode is much larger than for other Lamb modes. Numerical simulations show that the wavelength to thickness ratio ( $\lambda_0/d$ ) does not vary much with Poisson's ratio  $\nu$ . For the  $S_1$ -Lamb mode:  $\lambda_0/d$  varies from 3.4 to 5 as  $\nu$  varies from 0 to 0.4. Except for  $\nu$  values close to the limits where the ZGV resonance disappears, the optimal conditions are approximately fulfilled when the spot diameter is of the order of twice the plate thickness. So, for a 0.5-mm-thick Duralumin plate ( $\nu=0.34$ ), there is no need to focus the Nd:YAG laser beam.

## B. $S_1$ mode ZGV resonance

Since the acoustic energy of ZGV modes does not propagate, it is judicious to use superimposed source and detection points. However, the laser energy absorption heats the air in the vicinity of the surface and produces a variation of the optical index along the path of the probe beam. The resulting phase shift induces a very large low frequency voltage, which saturates the electronic detection circuit of the optical probe. This spurious thermal effect is eliminated by interposing a high-pass filter before the amplifying stage. The cutoff frequency of this filter was chosen equal to 1 MHz.

Experiments were carried out on a commercially available Duralumin plate of average thickness  $d=0.49$  mm and lateral dimensions equal to 100 and 150 mm. Figure 3 shows the fast Fourier transform of the first 300  $\mu\text{s}$  of the signal measured by the optical probe. The spread spectrum corresponds to the  $A_0$  Lamb mode. In the low frequency range, this flexural mode gives rise to large displacement amplitudes for the out-of-plane component. However, the prominent feature is a sharp peak at 5.86 MHz. From the theoret-

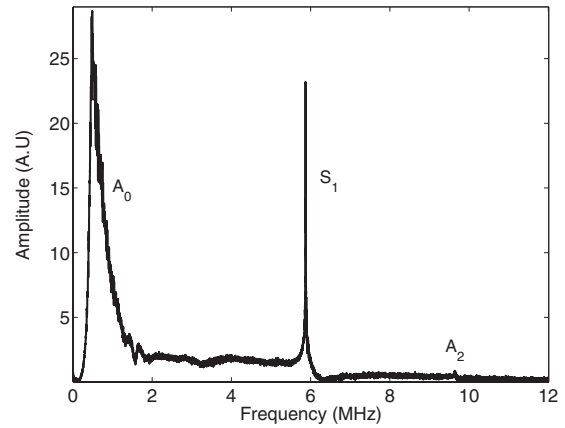


FIG. 3. Spectrum of the signal measured on a 0.49-mm-thick Duralumin plate.

ical dispersion curve of the  $S_1$  mode ( $f_0d=2.866$  MHz mm) and taking account of the average plate thickness, the resonance is expected to occur at a frequency  $f_0=5.85$  MHz, very close to the experimental value. The relative difference, smaller than 0.2%, can be ascribed to the uncertainty range in the material parameters and in the plate thickness. The small peak at 9.6 MHz corresponds to the thickness resonance at  $fd=4.71$  MHz mm of the  $A_2$  Lamb mode in Fig. 1.

## C. Backward-wave propagation and dispersion curves

As discussed in several papers,<sup>17,18</sup> at the ZGV frequency the  $S_1$  and  $S_{2b}$  modes interfere, having opposite wave vectors. In order to confirm the origin of this resonance, we have measured, with the aid of LBU techniques, the distribution of temporal and spatial frequencies of the out-of-plane displacement. The interference phenomena and the backward  $S_{2b}$  branch can be clearly identified by investigating the wave propagation along the Duralumin plate.

The laser source to probe distance  $r$  was varied from 0 to 10 mm in 10  $\mu\text{m}$  steps. At each source to receiver distance, the normal displacement  $u(r,t)$  was recorded during 300  $\mu\text{s}$  with a 50 MHz sampling frequency. The measured signals are time Fourier transformed into  $U(r,f)$ . In Fig. 4, the amplitude  $|U(r,f)|$  plotted for  $f$  varying from 5.85 to 5.93 MHz, reveals a standing mode due to the interference of two waves propagating in opposite directions, and generated with comparable amplitudes. The distance between adjacent nodes is equal to about half a wavelength of the  $S_1$  and  $S_{2b}$  modes ( $\lambda=V_0/f_0=1.92$  mm). It can be observed that the resonance frequency slightly increases with the distance to the source. At the ZGV resonance frequency  $f_0$  the acoustic energy does not propagate, and as Lamb modes at frequencies lower than  $f_0$  are evanescent, only propagative Lamb waves at frequencies higher than  $f_0$  contribute at distances from the source larger than  $\lambda_0$ .

This existence of counter propagative modes is confirmed by calculating the spatial Fourier transform  $\bar{U}(k,f) = \int U(r,f)e^{ikr}dr$ . The power spectrum is computed at a frequency (5.89 MHz) slightly higher than the ZGV resonance frequency, for which the modes are propagative. The spec-

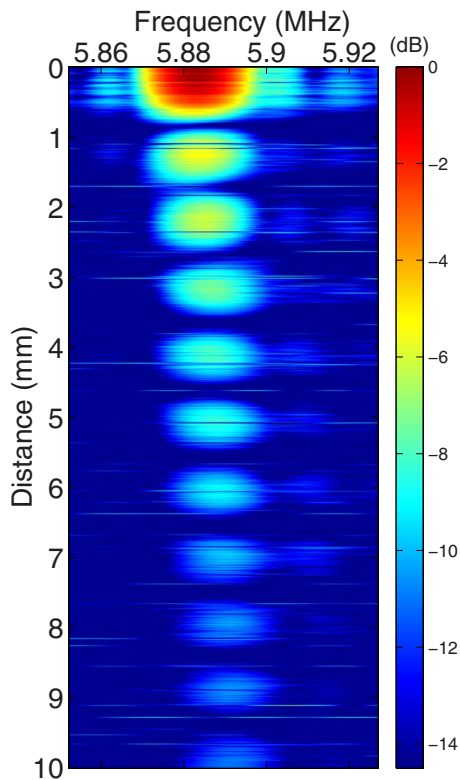


FIG. 4. (Color online) Spatial distribution of the displacement amplitude resulting from the interferences of the two counter-propagating waves  $S_1$  and  $S_{2b}$ .

trum, plotted in Fig. 5, is composed of two main peaks. The peak at a negative value of  $k$ , similar to the larger one in the positive wave number domain, clearly demonstrates the backward propagation. Due to the up-shift of the operating frequency, the positive and negative  $k$  values are not exactly opposite. The wave numbers ( $-2.95 \text{ mm}^{-1}$  and  $3.77 \text{ mm}^{-1}$ ) correspond to the expected ones for the  $S_1$  and  $S_{2b}$  modes around the ZGV point ( $k_0 d = 1.58$  and  $d = 0.49 \text{ mm} \rightarrow k_0 = 3.22 \text{ mm}^{-1}$ ). The other two peaks in Fig. 5 can be ascribed to the  $S_0$  and  $A_0$  Lamb modes.

Applying this signal processing in a large range of frequencies allows us to plot the dispersion curves. As previ-

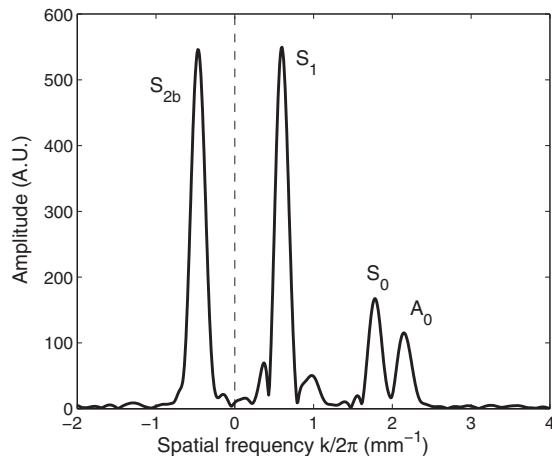


FIG. 5. Spatial Fourier transform of the normal displacement at 5.894 MHz. The negative wave number is clearly put in evidence.

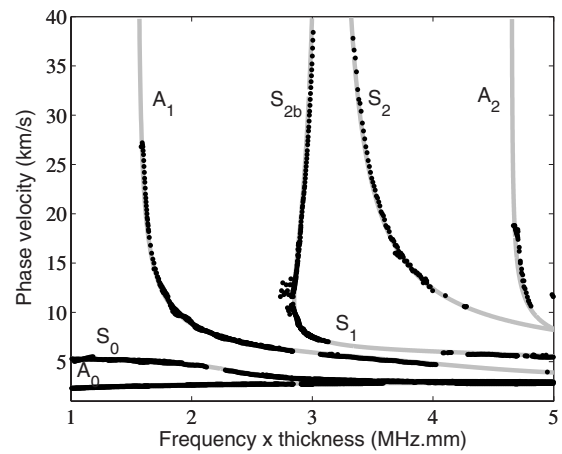


FIG. 6. Measured (dots) and predicted (continuous lines) dispersion curves for the 0.49-mm-thick Duralumin. The high velocity branches are obtained with the unfocused laser source, while the low phase velocity branches are obtained by focusing the laser beam.

ously indicated, the laser source beam was unfocused, providing a 1 mm spot size, approximately equal to half the  $S_1$  ZGV wavelength  $\lambda_0$ . This allows an efficient generation of this mode and of most modes of wavelength larger than 2 mm. In order to complete the dispersion curves with the modes of smaller wavelength, a second set of measurements was performed using a  $50 \mu\text{m}$  source diameter. At each temporal frequency, spatial Fourier transform was applied to the data taken over all spatial steps. The spatial frequencies of the laser generated acoustic modes were then determined by identifying the peaks in the power spectrum. The obtained dispersion curves are plotted in Fig. 6.

These experimental results highlight the main features of the  $S_1$ -ZGV Lamb mode, such as resonance effect, backward wave propagation, interference between backward and forward modes. Such an unusual behavior is often qualified as “anomalous.”<sup>23</sup> In fact, the occurrence of a ZGV mode is not a unique phenomenon. For an isotropic plate of any Poisson’s ratio, it exists in a large range of frequencies, involving nearly all the Lamb modes. In the next section, the conditions required for the existence of ZGV Lamb modes are investigated and an interpretation in terms of a strong repulsion between a pair of modes in the vicinity of the cutoff frequencies is proposed.

### III. EXISTENCE OF ZGV LAMB MODES

Elastic properties of an isotropic material are characterized by two constants  $c_{11}$  and  $c_{12}$ . However, Lamb wave propagation can be expressed in terms of only one dimensionless parameter, the bulk wave velocity ratio  $\kappa = V_L/V_T$  or the Poisson’s ratio  $\nu$ .

$$\nu = \frac{\kappa^2 - 2}{2(\kappa^2 - 1)}, \quad \text{with } \kappa = \sqrt{\frac{2(1-\nu)}{1-2\nu}}. \quad (1)$$

An important distinction in the behavior of plate modes occurs for small  $k$  values ( $kd \ll 1$ ). As shown in Fig. 1, only the fundamental modes  $A_0$  and  $S_0$  exhibit free propagation to zero frequency. The higher modes admit a cutoff frequency  $f_c$  for  $k=0$  and the dispersion curves start from the frequency

axis with a zero group velocity. However, these cutoff modes do not correspond to ZGV modes like the one discussed in the previous section for which  $k \neq 0$ .

At cutoff frequencies, multiple reflections of longitudinal or shear waves between the top and bottom faces of the plate give rise to a thickness shear resonance (modes  $S_{2n}$  or  $A_{2m+1}$ ) or to a thickness stretch resonance (modes  $S_{2m+1}$  or  $A_{2n}$ ). For symmetric modes, the even solutions are such that

$$f_c d = nV_T, \quad \text{mode } S_{2n} \quad (n \geq 1) \quad (2)$$

and the odd solutions are such that

$$f_c d = (2m+1)\frac{V_L}{2}, \quad \text{mode } S_{2m+1} \quad (m \geq 0), \quad (3)$$

where  $n$  and  $m$  are integers. For antisymmetric modes, the even solutions are such that

$$f_c d = nV_L, \quad \text{mode } A_{2n} \quad (n \geq 1) \quad (4)$$

and the odd solutions are such that

$$f_c d = (2m+1)\frac{V_T}{2}, \quad \text{mode } A_{2m+1} \quad (m \geq 0). \quad (5)$$

For example, in Fig. 1, the cutoff frequency of mode  $S_1$  occurs at  $V_L/2d$  and that of mode  $S_2$  at  $V_T/d$ . Following Ref. 24, the index of each Lamb mode in the previous classification and in Fig. 7 is equal to the number of nodes in the plate thickness both for shear (in-plane) displacements (modes  $S_{2n}$  and  $A_{2m+1}$ ) and normal (out-of-plane) displacements (modes  $S_{2m+1}$  and  $A_{2n}$ ). This numbering, different from that found in many textbooks, is fundamental for understanding the conditions of occurrence of the ZGV modes.

In the same family and for modes of different parity, the order of cutoff frequencies and then of dispersion curves depends on the bulk wave velocity ratio  $\kappa = V_L/V_T$ , i.e., on the Poisson's ratio  $\nu$ . For example, the curves for mode  $S_1$  and  $S_2$  interchange their relative positions for the critical values  $\kappa=2$  and  $\nu=1/3$ . This exceptional case, when two branches of the dispersion curves of the same symmetry intersect at cutoff, was first pointed out by Mindlin.<sup>25</sup> For  $\nu$  equal to  $1/3$ , the  $S_1$  and  $S_2$  branches intersect the frequency axis at the same point with nonzero slopes, of equal magnitude and opposite signs.<sup>17</sup>

In the following, we show that such coincidence of two cutoff frequencies plays a fundamental role in the existence of a ZGV mode corresponding to a minimum frequency  $f_0$  for a nonzero wave number  $k_0$ . Extensive numerical calculations have been performed in order to determine the ZGV modes versus Poisson's ratio  $\nu$ . For a shear wave velocity, arbitrarily chosen as  $V_T=3.0$  km/s, and a given Poisson's ratio varying by 0.001 step from 0 to 0.5, the longitudinal wave velocity  $V_L$  is computed. Using well-known Rayleigh-Lamb equations, the group velocity is calculated by numerical differentiation and the minimum frequencies  $f_0$  corresponding to ZGV points are determined by the zero crossings of the group velocity. Results are presented in Fig. 8 as a universal plot, first used by Meitzler<sup>17</sup> for the  $S_1$  and  $S_2$

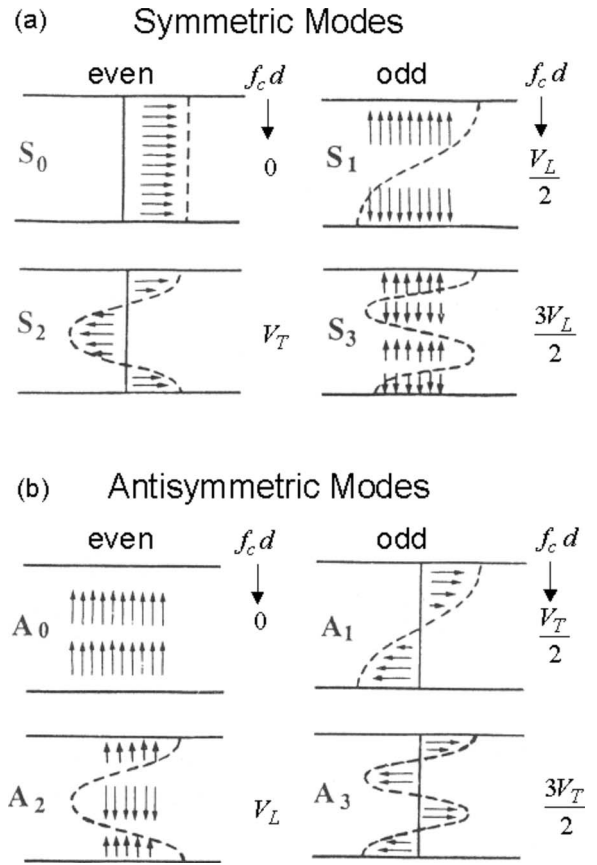


FIG. 7. Mechanical displacements and cutoff frequencies for the first few symmetric (a) and antisymmetric (b) Lamb modes in an isotropic plate of thickness  $d$ , for  $k=0$  (from Fig. 5.38, Ref. 24).

modes, of the dimensionless quantity  $F = fd/V_T$  (with  $f=f_0$  or  $f_c$ ) varying in the range  $0 \leq F \leq 5$ , versus Poisson's ratio in the usual range  $0 \leq \nu < 0.5$ .

According to Eqs. (2)–(5), horizontal lines at levels  $0.5, 1, 1.5, 2, \dots$ , correspond alternatively to cutoff frequencies of  $A_{2m+1}$  and  $S_{2n}$  Lamb modes and dashed curves labeled  $0.5V_L/V_T, V_L/V_T, 1.5V_L/V_T, \dots$ , correspond alternatively to cutoff frequencies of  $S_{2m+1}$  and  $A_{2n}$  Lamb modes. From the minimum frequency curves (thick lines) it appears that ZGV modes exist only in the vicinity of crossing points of cutoff frequency curves for modes belonging to the same family: symmetric or antisymmetric. The difference between the minimum frequency and the nearest cutoff frequency is the largest at the coincidence points. These observations lead to explain the ZGV phenomenon as resulting from a strong repulsion between a pair of modes in the vicinity  $k=0$ . The smaller the frequency gap at  $k=0$ , the stronger the repulsion.

For example, let us consider a pair of symmetric modes of different parity like  $S_5$  and  $S_8$ . As shown in Fig. 9, the difference between their cutoff frequencies, respectively  $2.5V_L/d$  and  $4V_T/d$ , depends on the Poisson's ratio  $\nu$ . For  $\nu=0.13$ , this difference is relatively large and the modes are weakly interacting [Fig. 9(a)]. For  $\nu=0.155$ , a stronger interaction leads to a nearly flat lower branch [Fig. 9(b)]. Since the wave velocity ratio is equal to the critical value  $\kappa=1.6$  for  $\nu=0.179$ , the cutoff modes are degenerated and the very strong repulsion creates a zero group velocity mode in the lower branch at  $k=k_0$  [Fig. 9(c)], similar to the one observed

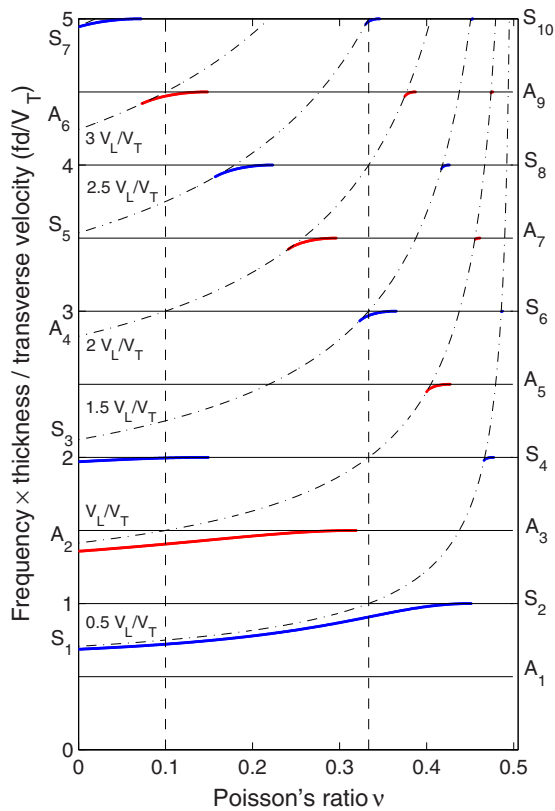


FIG. 8. (Color online) Dimensionless cutoff frequencies  $f_c d / V_T$  (horizontal lines) and  $f_0 d / V_T$  (dashed curves) and minimum frequency  $f_0 d / V_T$  versus the Poisson's ratio in the range  $0 \leq \nu \leq 0.5$ . The ZGV branches (thick lines) appear about crossing points of cutoff frequency curves for modes belonging to the same family: symmetric or antisymmetric. Vertical dashed lines correspond to the critical values  $\nu_1 = 1/3$  and  $\nu_2 = 1/10$ .

in Fig. 1. For  $\nu = 0.20$ , the  $S_5$ -mode cutoff frequency passes beyond the  $S_8$ -mode ones and the weaker coupling gives rise to a less pronounced trough [Fig. 9(d)].

Due to the symmetry through the median  $xy$  plane of the plate, symmetric and antisymmetric Lamb modes are uncoupled for any  $k$ . A dispersion curve for a symmetric (antisymmetric) mode may cross a curve for an antisymmetric (symmetric) mode. It is not the case for modes belonging to the same family.<sup>26</sup> However, in Fig. 7 it can be observed that

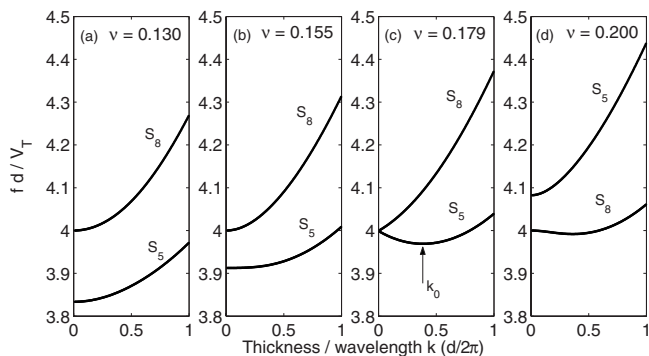


FIG. 9. Dispersion curves of  $S_5$  and  $S_8$  modes for selected Poisson's ratio  $\nu$ . (a) Weakly interacting modes. (b) Stronger interaction leading to a nearly flat lower branch. (c) Poisson's ratio such as the cutoff modes degenerate ( $\kappa = 1.6$ ): the very strong repulsion creates a zero group velocity mode at  $k = k_0$ . (d)  $S_5$  and  $S_8$  cutoff frequencies separate: The weaker repulsion gives rise to a less pronounced trough.

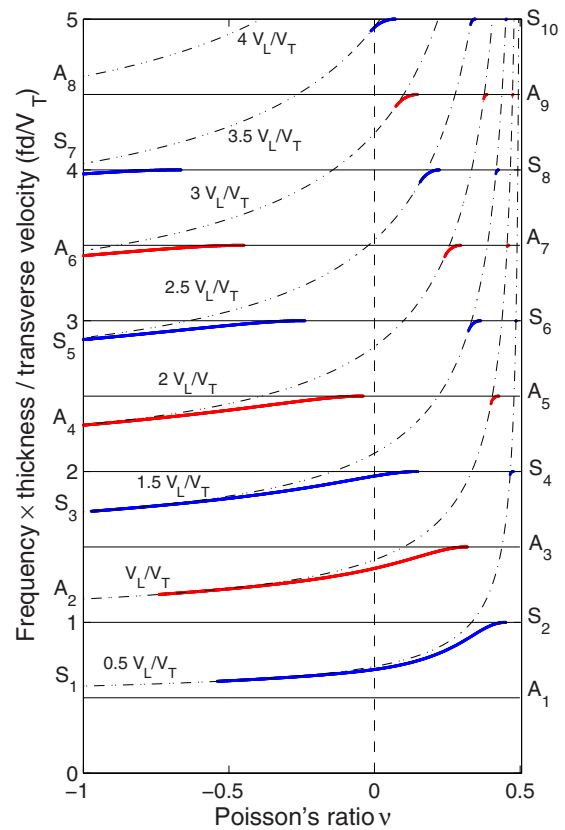


FIG. 10. (Color online) Dimensionless cutoff frequencies and minimum frequency of Lamb modes versus the Poisson's ratio in the physical range  $-1 \leq \nu \leq 0.5$ . The third ZGV branch results from the coupling between  $S_3$  and  $S_4$  Lamb modes for a negative Poisson's ratio  $\nu = -1/7$ .

for  $k=0$  even and odd modes of the same family are also uncoupled. This property is general because it has its origin in the reflection symmetry through the transverse  $yz$  plane, shared for  $k=0$  by any waveguide uniform along the  $x$ -propagation direction.<sup>27</sup> Then the difference between cutoff frequencies of a pair of symmetric (antisymmetric) Lamb modes can be made arbitrarily small. For a nonzero wave number, the propagation along the  $+x$  or  $-x$  direction breaks this symmetry. Odd and even modes belonging to the same family are not yet orthogonally polarized. Both longitudinal and transverse components are involved in the mechanical displacement of each mode, introducing a wave coupling. This phenomenon leads to a strong repulsion between the dispersion curves of the two neighboring modes, responsible of the negative-slope region and zero group velocity point of the lower branch in Figs. 9(c) and 9(d).

From these considerations, the following rules for selecting ZGV modes can be stated:

- 1- since symmetric and antisymmetric modes are uncoupled for any wave number, the ZGV phenomenon occurs only between modes of the same family,
- 2- in the same family no coincidence exists between cutoff frequencies of modes having the same parity, then ZGV modes results only from the repulsion between  $S_{2m+1}$  and  $S_{2n}$  Lamb modes or  $A_{2n}$  and  $A_{2m+1}$  Lamb modes,
- 3- for symmetric ZGV modes, the repulsion, i.e., the difference  $f_0 - f_c$ , is maximum for the critical Poisson's ratio  $\nu$  given by Eq. (1) with:

TABLE I. Symmetric Lamb modes (frequency thickness product  $fd < 5V_T$ ). Critical bulk wave velocity ratio  $V_L/V_T$  and Poisson's ratio  $\nu$  for the 12 ZGV modes plotted in Fig. 8.

Symmetric ZGV modes	$S_3/S_4$	$S_7/S_{10}$	$S_5/S_8$	$S_5/S_{10}$ $S_3/S_6$ $S_1/S_2$	$S_3/S_8$	$S_3/S_{10}$	$S_1/S_4$	$S_1/S_6$	$S_1/S_8$	$S_1/S_{10}$
$V_L/V_T$	4/3	10/7	8/5	2	8/3	10/3	4	6	8	10
$\nu$	-0.1429	0.0196	0.1795	0.3333	0.4182	0.4505	0.4667	0.4857	0.4921	0.4949

$$\kappa_S = \left( \frac{V_L}{V_T} \right)_S = \frac{2n}{2m+1}, \quad (6)$$

4- for antisymmetric ZGV modes, the repulsion is maximum for the critical bulk wave velocity ratio:

$$\kappa_A = \left( \frac{V_L}{V_T} \right)_A = \frac{2m+1}{2n}. \quad (7)$$

$\kappa_A$  and  $\kappa_B$  are rational numbers, that is, ratios of even integers to odd integers.

For the first symmetric ZGV mode ( $m=0, n=1 \rightarrow \kappa_{S1}=2$ ) the repulsion between the  $S_1$  and  $S_2$  Lamb modes is maximum for  $\nu_1=1/3$ . For the first antisymmetric ZGV mode ( $m=1, n=1 \rightarrow \kappa_{A2}=3/2$ ) the repulsion between the  $A_2$  and  $A_3$  Lamb modes is maximum for  $\nu_2=1/10$ . As pointed out by Negishi,<sup>28</sup> the existence range of these so-called  $S_1$  and  $A_2$ -ZGV modes are relatively wide with extinction points of  $\nu=0.45$  and  $0.32$ , respectively. As shown in Fig. 8, higher order ZGV modes exist over narrower ranges of Poisson's ratio  $\nu$  and frequency  $\times$  thickness product  $fd$ . It should be noted that symmetric ( $S_3/S_6$  or  $S_5/S_{10}$ ) and antisymmetric ( $A_6/A_9$ )-ZGV modes correspond to the same values  $\nu_1$  and  $\nu_2$  than fundamental ( $S_1/S_2$ ) and ( $A_2/A_3$ )-ZGV modes, respectively. The reason is that the indices of the pair of modes are multiplied by an odd number, 3 or 5, leading to unchanged bulk wave velocity ratio:  $\kappa_{S1}=2$  and  $\kappa_{A2}=3/2$ . Such high order ZGV modes can be considered as harmonics of the fundamental ones  $S_1/S_2$  and  $A_2/A_3$ .

For  $\nu < 0.14$ , a minimum frequency is exhibited in Fig. 8, just below the cutoff frequency ( $fd=2V_T$ ) of the  $S_4$  mode. It can be predicted that this branch corresponds to the coupling with the  $S_3$  mode. According to Eq. (1), the bulk wave velocity ratio  $\kappa=4/3$  leads to a negative Poisson's ratio  $\nu=-1/7$ . As shown in Fig. 10, where the minimum frequencies are plotted in the whole physical range of Poisson's ratio from  $-1 \leq \nu < 0.5$ , other ZGV modes with cutoff frequency coincidences for negative  $\nu$  values have no extension in the usual material range from  $0 \leq \nu < 0.5$ .

Limiting the frequency thickness product  $fd$  to  $5V_T$  and for  $0 \leq \nu < 0.5$ , 12 symmetric ZGV modes can be found in Fig. 8. The critical values of the bulk wave velocity ratio and of the Poisson's ratio are given in Table I. The ranges of

existence  $[\nu_{\min} \nu_{\max}]$  of these modes are gathered in Table II. In the same domain of variations for  $fd$  and  $\nu$ , only seven antisymmetric ZGV modes exist. Their characteristics are given in Tables III and IV.

It should be noted that Eq. (6) was given by Werby and Überall for symmetric Lamb modes.<sup>23</sup> However, these authors developed only the simplest case  $V_L=2V_T$ , reported earlier,<sup>25</sup> and many of their conclusions concerning the existence and the extinction points of ZGV Lamb modes are in contradiction with results of the present work.

Then, in an isotropic plate, the existence of zero group velocity modes is not a rare phenomenon. All Lamb modes, except the first three  $S_0$ ,  $A_0$ , and  $A_1$ , exhibit such a behavior. This effect, which cannot be qualified as "anomalous" as it is often the case in the literature, is predicted by using simple rules. Since the negative slope branches in the dispersion curves result from a strong repulsion, in the vicinity of the cutoff frequencies, between two modes having the same symmetry, the frequency minima always occur for small wave numbers. According to this physical meaning, ZGV modes should be labeled with the name of the two coupled Lamb modes:  $S_{2m+1}/S_{2n}$  for the symmetric ones and  $A_{2n}/A_{2m+1}$  for the antisymmetric ones.

In the next section, using LBU techniques, we investigate the local vibrations of an elastic plate of uniform thickness and we establish a link between the experimental resonance spectrum and the predicted ZGV Lamb modes.

#### IV. LOCAL RESONANCE SPECTRUM OF A PLATE AND MATERIAL CHARACTERIZATION

Local resonance techniques, such as the "Impact Echo" method developed for concrete applications, are of a great interest for nondestructive evaluation of materials. Therefore it is important to understand the transient response of a slab-like structure to a mechanical or a laser impact. The term "local resonance" means that the distance between the source and the detector is less than the wavelength. At higher frequencies and in our experiments using LBU techniques, the lateral extension of the source is of the order of the plate thickness and the point-like detection is localized in the source area.

TABLE II. Range of existence versus Poisson's ratio  $[\nu_{\min} \nu_{\max}]$  for the first ten symmetric ZGV Lamb modes.

ZGV mode	$S_3/S_4$	$S_7/S_{10}$	$S_5/S_8$	$S_1/S_2$	$S_3/S_6$	$S_5/S_{10}$	$S_3/S_8$	$S_3/S_{10}$	$S_1/S_4$	$S_1/S_6$
$\nu_{\min}$	-0.973	-0.012	0.156	-0.540	0.323	0.330	0.417	0.451	0.466	0.485
$\nu_{\max}$	0.149	0.072	0.223	0.451	0.365	0.346	0.426	0.453	0.477	0.487

TABLE III. Antisymmetric Lamb modes (frequency thickness product  $fd < 5V_T$ ). Critical bulk wave velocity ratio  $V_L/V_T$  and Poisson's ratio  $\nu$  for the seven ZGV Lamb modes plotted in Fig. 8.

Antisymmetric ZGV modes	$A_6/A_9$ $A_2/A_3$	$A_4/A_7$	$A_4/A_9$	$A_2/A_5$	$A_2/A_7$	$A_2/A_9$
$V_L/V_T$	3/2	7/4	9/4	5/2	7/2	9/2
$\nu$	0.1000	0.2576	0.3769	0.4048	0.4556	0.4740

Experiments have been performed according to the procedure described in Sec. II A on plates of thickness  $d$  in the millimeter range, made of various materials (steel, nickel, zinc, fused silica and Duralumin). The time Fourier transform was computed with the first 60  $\mu\text{s}$  of the signals measured by the optical probe at the same point. Figure 11 shows the relative magnitude of the frequency spectrum (in dB) versus the frequency normalized to the shear wave velocity (vertical scale:  $F = fd/V_T$ ) for two of them: fused silica and Duralumin. The central part in Fig. 11 reproduces the theoretical ZGV branches in the range  $0 \leq F \leq 5$ . The upper limit corresponds to the higher frequencies in the laser pulse spectrum ( $f_{\text{max}} \cong 15$  MHz), the plate thickness ( $d \cong 1$  mm) and the transverse wave velocity ( $V_T \cong 3$  km/s). Vertical dotted lines are drawn for the Poisson's ratio of fused silica (on the left) and Duralumin (on the right). In both cases, each intersection of these lines with a ZGV branch corresponds to a clear resonance peak. Taking into account that for Duralumin the Poisson's ratio  $\nu = 0.338$  is very close to the critical value  $\nu_1 = 1/3$ , the first, third, and fourth peaks correspond to the fundamental ( $S_1/S_2$ )-ZGV mode and to its harmonics  $S_3/S_6$  and  $S_5/S_{10}$  (see Table I). The second one at  $F = 1.5$ , for which the intersection is close to the extinction point of the ( $A_2/A_3$ )-ZGV mode, is less intense than the other peaks for which the intersection nearly coincides with the maximum repulsion between the coupled modes. For fused silica ( $\nu = 0.172$ ) the first and second peaks are of the same order of magnitude. The third one, at  $F = 2$ , is weak since the intersection lies outside the zone of existence of the ( $S_3/S_4$ )-ZGV mode.

Similar results obtained with other materials lead to the conclusion that *the local resonance spectrum of a plate is entirely governed by the zero-group-velocity Lamb modes*. This conclusion is based on two points: first, the high excitability of such ZGV modes by a laser source of lateral dimensions of the order of the plate thickness. Second, the energy of other laser-excited Lamb modes flows outside the source area, at their nonzero group velocity, in less than 1  $\mu\text{s}$ . Then, only ZGV modes, trapped under the source, give rise to a local vibration of the plate detectable over a long time.

For a given pair of Lamb modes, the ZGV resonance frequency  $f_0$  is slightly smaller than the cutoff frequency  $f_c$ :

$$f_0 = \beta f_c \quad \text{with} \quad f_c = p \frac{V}{2d}, \quad (8)$$

where  $p$  is an integer and  $V$  is equal to  $V_L$  or  $V_T$ , according to Eqs. (2)–(5). The dimensionless parameter  $\beta$  was first incorporated as a “shape factor” in the American Society for Testing and Materials standards in order to correct the wall thickness measured by the impact echo method.<sup>4</sup> Its value, less than unity, depends only on the Poisson's ratio  $\nu$ .<sup>12</sup>

For a given homogeneous material, the resonance frequency is sensitive to the plate thickness  $d$ . We have shown that relative variations as small as 0.02% can be measured, without any mechanical contact, from the shift of the resonance frequency of the  $S_1$  ZGV mode.<sup>15</sup> The lateral resolution, in the millimeter range, is one order of magnitude better than the one obtained with electromagnetic acoustic transducers.<sup>5</sup> Moreover, the ZGV resonance method is not limited to metallic materials.

The material damping can be also estimated from the half-power bandwidth  $\Delta f_0$  of the resonance peak and from the phase velocity  $V_0$  at the ZGV point. Assuming a viscoelastic mechanism, the attenuation coefficient  $\alpha$  ( $\text{m}^{-1}$ ) is related to the acoustic quality factor  $Q = f_0/\Delta f_0$ :

$$\alpha = \frac{k_0}{2Q} = \pi \frac{\Delta f_0}{V_0}. \quad (9)$$

For an accurate determination of the attenuation coefficient, the signal acquisition time window must be larger than the inverse of the bandwidth. This method, first applied with the  $S_1$  mode,<sup>15</sup> can be extended to other ZGV modes, providing the attenuation coefficient at higher frequencies.

Figure 11 and experiments performed on other materials show that many ZGV resonances can be excited in a single shot and detected locally on a plate. The ratio of two resonance frequencies is independent of the plate thickness  $d$ . It depends only on the Poisson's ratio  $\nu$ , the value of which can be determined accurately from frequency measurements. Using LBU techniques, this method has been tested on a large number of isotropic materials. The Poisson's ratio and the bulk wave velocities were determined locally in thin plates or shells.<sup>16</sup> In these experiments, only the first two resonances at the minimum frequencies of  $S_1$  and  $A_2$  Lamb

TABLE IV. Antisymmetric ZGV Lamb modes. Range of existence versus Poisson's ratio [ $\nu_{\text{min}}$   $\nu_{\text{max}}$ ].

ZGV mode	$A_2/A_3$	$A_6/A_9$	$A_4/A_7$	$A_4/A_9$	$A_2/A_5$	$A_2/A_7$	$A_2/A_9$
$\nu_{\text{min}}$	-0.740	0.073	0.241	0.375	0.400	0.455	0.474
$\nu_{\text{max}}$	0.319	0.148	0.296	0.387	0.427	0.461	0.476

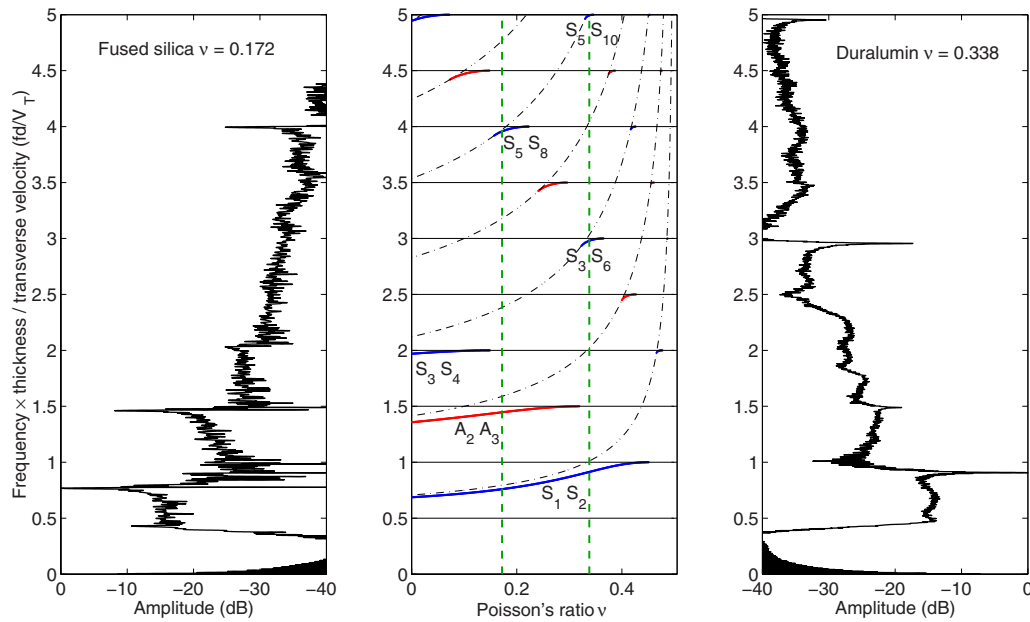


FIG. 11. (Color online) Local vibration spectrum of a fused silica plate of thickness  $d=1.1$  mm (on the left) and of a Duralumin plate of thickness  $d=1.0$  mm (on the right). Resonance peaks occur at the intersection of the minimum frequency curves of Lamb modes, plotted in the central part. The vertical dotted lines correspond to the Poisson's ratio of fused silica ( $\nu=0.172$ ) and of Duralumin ( $\nu=0.338$ ).

modes are used. From the previous analysis, it is clear that this characterization method can be generalized to higher order ZGV modes. Taking into account these modes having a narrow range of existence (see Tables II and IV) for the correlation between the experimental and theoretical local resonance spectra would dramatically improve the determination of the elastic parameters.

It should be recalled that in all experiments, the vibrations are excited locally in the thermoelastic regime and that the measurements are performed on the same face of the sample, without any mechanical contact.

## V. CONCLUSION

Using laser-based ultrasonic techniques, we have experimentally investigated the resonance and ringing effects associated with the  $S_1$  ZGV Lamb mode in an isotropic plate. The spatial distribution of the mechanical displacement has been optically measured on the surface of the plate. The spatial Fourier transform, computed at the ZGV resonance frequency, exhibits two peaks for opposite wave numbers. Backward and forward wave propagation, clearly revealed in these experiments, explained the observed standing wave pattern.

We developed a simple analysis based on the coincidences of Lamb modes cutoff frequencies, which demonstrates that the occurrence of zero group velocity (ZGV) Lamb modes is not a rare phenomenon. Numerical calculations show that the frequency  $\times$  thickness product undergoes a minimum in a range of Poisson's ratio about the critical value for which the cutoff frequency curves of modes of similar symmetry intercept. An interpretation of this phenomenon in terms of mode coupling has been given. Using a classification where the index of each mode is equal to the number of nodes at the cutoff frequency in the plate thick-

ness, ZGV Lamb modes result from the coupling of a pair of modes having a different parity, such as  $S_{2m+1}$  and  $S_{2n}$  or  $A_{2n}$  and  $A_{2m+1}$ .

Vibrational spectra measured on plates made of various materials lead to the conclusion that the local resonance spectrum of an unloaded elastic plate is entirely governed by the zero-group-velocity Lamb modes. We indicate how these ZGV resonances can be exploited for measuring the plate thickness, the attenuation coefficient, the Poisson's ratio, and the bulk wave velocities of thin plates. Since the vibrations are excited in the thermoelastic regime by a laser pulse and detected at the same point by an optical interferometer, these measurements are local and performed in a single shot on the same face of the plate, without any mechanical contact. Moreover, this ZGV resonance method, based on frequency measurements, is very accurate. ZGV modes have also been observed in anisotropic or multilayered plates and in cylindrical shells. We expect that most results presented in this paper can be generalized to these various structures.

<sup>1</sup>L. C. Lynnworth, *Ultrasonic Measurements for Process Control: Theory, Techniques Applications* (Academic, Boston, 1989).

<sup>2</sup>P. Cawley, M. J. S. Lowe, D. N. Alleyne, B. Pavlakovic, and P. Wilcox, "Practical long range guided wave testing: Applications to pipes and rail," *Mater. Eval.* **61**, 66–74 (2003).

<sup>3</sup>W. Gao, C. Glorieux, and J. Thoen, "Laser ultrasonic study of Lamb waves: Determination of the thickness and velocities of a thin plate," *Int. J. Eng. Sci.* **41**, 219–228 (2003).

<sup>4</sup>M. Sansalone and N. J. Carino, "Impact echo: A method for flaw detection in concrete using transient stress waves," Report No. NBSIR86-3452, National Bureau of Standards, Gaithersburg, MD (1986).

<sup>5</sup>S. Dixon, C. Edwards, and S. B. Palmer, "High accuracy non-contact ultrasonic thickness gauging of aluminium sheet using electromagnetic acoustic transducers," *Ultrasonics* **39**, 445–453 (2001).

<sup>6</sup>I. A. Viktorov, *Rayleigh and Lamb Waves* (Plenum, New York, 1967).

<sup>7</sup>J. D. Achenbach, *Wave Propagation in Elastic Solids* (North-Holland, Amsterdam, 1980).

<sup>8</sup>I. Tolstoy and E. Usdin, "Wave propagation in elastic plates: Low and high mode dispersion," *J. Acoust. Soc. Am.* **29**, 37–42 (1957).

- <sup>9</sup>R. L. Weaver and Y.-H. Pao, "Spectra of transient waves in elastic plates," *J. Acoust. Soc. Am.* **72**, 1933–1941 (1982).
- <sup>10</sup>T. Liu, W. Karunasena, S. Kitipornchai, and M. Veidt, "The influence of backward wave transmission on quantitative ultrasonic evaluation using Lamb wave propagation," *J. Acoust. Soc. Am.* **107**, 306–314 (2000).
- <sup>11</sup>D. Holland and D. E. Chimenti, "High contrast air-coupled acoustic imaging with zero group velocity Lamb modes," *Appl. Phys. Lett.* **83**, 2704–2706 (2003).
- <sup>12</sup>A. Gibson and J. S. Popovics, "Lamb wave basis for impact-echo method analysis," *J. Eng. Mech.* **131**, 438–443 (2005).
- <sup>13</sup>C. Prada, O. Balogun, and T. W. Murray, "Laser based ultrasonic generation and detection of zero-group velocity Lamb waves in thin plates," *Appl. Phys. Lett.* **87**, 194109 (2005).
- <sup>14</sup>O. Balogun, T. Murray, and C. Prada, "Simulation and measurement of the optical excitation of the S1 zero group velocity Lamb wave resonance in plate," *J. Appl. Phys.* **102**, 064914 (2007).
- <sup>15</sup>D. Clorennec, C. Prada, D. Royer, and T. W. Murray, "Laser impulse generation and interferometer detection of zero-group velocity Lamb modes," *Appl. Phys. Lett.* **89**, 024101 (2006).
- <sup>16</sup>D. Clorennec, C. Prada, and D. Royer, "Local and noncontact measurement of bulk acoustic wave velocities in thin isotropic plates and shells using zero-group velocity Lamb modes," *J. Appl. Phys.* **101**, 034908 (2007).
- <sup>17</sup>A. H. Meitzler, "Backward-wave transmission of stress pulses in elastic cylinders and plates," *J. Acoust. Soc. Am.* **38**, 835–840 (1965).
- <sup>18</sup>J. Wolf, T. D. K. Ngoc, R. Kille, and W. G. Mayer, "Investigation of Lamb waves having negative group velocity," *J. Acoust. Soc. Am.* **83**, 122–126 (1988).
- <sup>19</sup>G. Kaduchak, D. H. Hughes, and P. L. Marston, "Enhancement of the backscattering of high-frequency tone bursts by thin spherical shells associated with a backwards wave: Observations and ray approximation," *J. Acoust. Soc. Am.* **96**, 3704–3714 (1994).
- <sup>20</sup>P. L. Marston, "Negative group velocity Lamb waves on plates and applications to the scattering of sound by shells," *J. Acoust. Soc. Am.* **113**, 2659–2662 (2003).
- <sup>21</sup>M. A. Biot, "General theorems on the equivalence of group velocity and energy transport," *Phys. Rev.* **105**, 1129–1137 (1957).
- <sup>22</sup>D. Royer and E. Dieulesaint, *Proceedings of the 1986 IEEE Ultrasonics Symp.* (IEEE, New York, 1986), p. 527.
- <sup>23</sup>M. F. Werby and H. Überall, "The analysis and interpretation of some special properties of higher order symmetric Lamb waves: The case for plates," *J. Acoust. Soc. Am.* **111**, 2686–2691 (2002).
- <sup>24</sup>D. Royer and E. Dieulesaint, *Elastic Waves in Solids 1: Free and Guided Propagation* (Springer, Berlin, 1999), p. 317.
- <sup>25</sup>R. D. Mindlin, *An Introduction to the Mathematical Theory of Vibrations of Elastic Plates*, U.S. Army Signal Corps Eng. Lab., Ft Monmouth, N. J., Monograph. Sec. 2.11 (1955). Edited by, J. Yang (World Scientific, Singapore, 2006).
- <sup>26</sup>B. Auld, *Acoustic Fields and Waves in Solids* (Wiley Interscience, New York, 1973), Vol. **II**, p. 81.
- <sup>27</sup>M. Ibanescu, S. G. Johnson, D. Roundy, C. Luo, Y. Fink, and J. D. Joannopoulos, "Anomalous dispersion relations by symmetry breaking in axially uniform waveguides," *Phys. Rev. Lett.* **92**, 063903 (2004).
- <sup>28</sup>K. Negishi, "Existence of negative group velocity in Lamb wave," *Jpn. J. Appl. Phys., Part 1* **26**, Supplement 26-1, 171–173 (1987).